Characterisation of interaction between combustion dynamics and equivalence ratio oscillations in a pressurised combustor

Jaap F. van Kampen and Jim B.W. Kok

University of Twente, Department of Thermal Engineering

P.O. Box 217, 7500 AE Enschede, The Netherlands

Received September 04, 2009; In revised form on January 13, 2010 and May 04, 2010; Accepted on May 16, 2010

ABSTRACT

In regular operation, all gas turbine combustors have a significant spontaneous noise level induced by the turbulent high power flame. This noise is characteristic for the operation as it is the result of the interaction between turbulence and combustion. Pressure fluctuations may also be generated by thermoacoustic instabilities induced by amplification by the flame of the acoustic field in the combustor. This paper focuses on the characterisation of the latter process, the combustion dynamics, in a pressurized premixed natural gas combustor. In order to predict the thermo-acoustically unstable operating ranges of modern gas-turbines with the use of an acoustic network model, it is essential to determine accurately the flame transfer function. This transfer function gives the relationship between a perturbation upstream of the flame and its combustion response, leading to acoustic forcing. In this paper, the flame transfer function is obtained by experimental means in a combustor test rig. This test rig was built in the framework of the European DESIRE project, and has the ability to perform thermo-acoustic measurements up to an absolute pressure of 5 bars. The maximum power of the setup is 500 kW.

The paper presents a method to determine the flame transfer function by factorizing it in six subfunctions. Systematically these subfunctions are determined. With the method presented, acoustic measurements on the steady, unperturbed flame and on the unsteady, actively perturbed flame are performed. The effect of pressure is investigated. The steady measurements are used to provide an acousto-combustion finger print of the combustor. In the unsteady measurements, the flame transfer function is reconstructed from the measured acoustic pressures. These flame transfer functions are compared to transfer functions obtained from a numerical experiment in CFD. Good agreement is obtained.

NOMENCLATURE

c	Speed of sound	[m/s]
f	Frequency	[1/s]

H	Transfer function between rate of heat release and mass flow	[–]
i	Square root of minus 1	[–]
L	Length	$[m]$
m	Mass flow	$[kg]$
M	Acoustic source term due to combustion dynamics	$[kg/(s^2m^3)]$
n	Normal vector of unity length	[–]
P	Pressure	$[kg/(m^2s)]$
q	Local thermal heat input to the gas per unit volume	$[kg/(s^2m)]$
Q	Total thermal heat input	$[kg/(s^2m)]$
R	Reflection coefficient	[–]
S	Surface area, spectral density	$\left[m^2\right]$, $ampl^2.s$
t	Time	$[s]$
T	Temperature	$[K]$
$\underline{u}$	Velocity vector	$[m/s]$
V	Volume	$[m^3]$
x	Axial coordinate	$[m]$

GREEK SYMBOLS

δ	Displacement of the MOOG valve piston	$[m]$
γ	Ratio of specific heat capacities at constant pressure and volume	[–]
ρ	Density of fluid	$[kg/(m^3)]$
ω	Radial frequency	$[rad/s]$
φ	Equivalence ratio, angular phase shift	[–], $[rad]$
τ	Viscous stress tensor	$[kg/(m^2s)]$
Δ	Perturbation	[–]
ζ	Impedance	$[kg/(m^2s)]$
λ	Wave length	$[m]$

SUBSCRIPTS

air	Air
e	Excess (density)
eq	Period of the fluctuating heat release rate equals flame residence time
exc	Excited
f1,f2, etc	Number of the factorization function (not a dimensionless function)
f	Fuel
flame	Volume of the flame
gas	Gas
in	Flow in to control volume
o	Reference state
meas	Measured
out	Flow out of control volume
x	Location

SUPERSCRIPTS

~ Favre averaging
- Time averaging
‘ Fluctuation of a variable per time unit
. Rate of input of a variable per time unit

1. INTRODUCTION

The search for more efficient and clean combustion systems has increased the interest in the subject of thermo-acoustic instabilities. A thermo-acoustic instability can be described as a feedback loop caused by the interaction between heat release fluctuations and sound, which results in a build up of acoustic pressure oscillations with time. The interest in these instabilities is mainly driven by the desire to decrease the levels of nitrogen oxides (NO_x). NO_x is mainly produced when the temperature at which combustion of natural gas takes place is relatively high. The combustion temperature can be lowered by burning a leaner mixture, i.e. a mixture with an excess of air compared to fuel. This mixture must be well premixed to prevent local variations of the fuel-to-air ratio and therefore locally higher temperatures. This concept is applied in the new generation of combustion systems for gas turbines, which are indicated as lean premixed combustion systems. The downside of these combustion systems is that they are prone to thermo-acoustically induced combustion instabilities. The high levelled acoustic pressure oscillations occurring with a thermo-acoustic instability impose an extra mechanical load on the wall of the combustor, which is usually called the liner. Additionally, heat transfer to the liner is augmented and local overheating may be induced.

The effect of the acoustic pressure oscillations on the structure and the consequences on the liner design play a crucial role with respect to the reliability of the gas turbine engine. To investigate this effect, the project DESIRE (Design and demonstration of highly reliable low NO_x combustion systems for gas turbines) was funded by the EC. The partners in the DESIRE project were Siemens Power Generation (initiator and coordinator), DLR, KEMA, E.ON, CERFACS, CIMNE and the University of Twente. The primary objective of DESIRE was to provide models for predicting the interaction between the sound produced by the flame and the resulting vibrations of the liner. The developed models are validated in an experimental setup built at the University of Twente. This UT-DESIRE test rig has a maximum thermal power of 500 kW at 5 bars absolute pressure. Therefore it is closer to realistic gas turbine conditions than most other experimental combustion set-ups. At the mentioned pressure and power, most thermo-acoustic experimental techniques seen in literature are available, such as dynamic pressure measurements, Planar Laser Induced Fluorescence (PLIF) OH, chemiluminescence CH*, active flame perturbation etc. Additionally, the setup distinguishes itself by the fact that it allows the measurement of the dynamic liner vibration as a response to the acoustic field generated by the flame. With these measurements, the complete coupled dynamic system of thermo-acoustic behaviour of the flame, the acoustic field and the structural vibrations of the liner can be studied.

The DESIRE project resulted in various publications. Steady and unsteady (i.e. the flame is actively perturbed) flame behaviour has been measured in the UT-DESIRE test rig with laser techniques as PLIF and chemiluminescence. This data is compared to results of LES simulations performed by CERFACS by Sengissen et al. (2007). Furthermore, the acousto-elastic measurements performed on the UT-DESIRE test rig can be found in the Ph.D thesis of Huls (2006). This Ph.D thesis also discusses modelling approaches to predict the vibration of the liner under steady and unsteady flame conditions. In the Ph.D thesis of Van Kampen (2006), the flame component and the prediction of instabilities in a combustion system is discussed. In this thesis, efficient measurement techniques and numerical algorithms to check combustion systems for their sensitivity to combustion instabilities are developed and validated.

This paper is partly based on the work discussed in Van Kampen (2006) and focusses on the acoustic measurements performed on the UT-DESIRE test rig. These acoustic measurements were intended to reconstruct the so-called flame transfer function (FTF) of the flame. This frequency-dependent transfer function represents the relationship between an applied perturbation upstream of the flame and the response of the flame in terms of the heat release rate. This is generally considered to be the main sound output of a flame (Crighton et al. (1992)).

The paper starts in Section 2 with an overview of the literature on acoustic measurements performed on experimental combustion setups. In Section 3, the interaction process between combustion and pressure fluctuations is discussed. In Section 4 a generic method for the measurement of the flame transfer function is presented. This function describes the interaction between combustion and pressure fluctuations. Section 5 gives a description of the UT-DESIRE setup, diagnostics and method of measurement. Subsequently, flame transfer functions determined by unsteady measurements are presented in Section 6. In these unsteady measurements, the fuel mass flow is perturbed, which indirectly perturbs the equivalence ratio.

The paper presents in Section 4 a new method to determine the flame transfer function for fuel mass flow variations, by factorizing it in 6 subfunctions. Systematically these subfunctions are determined. Three of these subfunctions can be evaluated from thermodynamics. One subfunction is the acousto-combustion fingerprint of the system and can be determined from a time registration of the steady state flame. Another subfunction characterizes the acoustic behaviour of the fuel line. This is obtained by means of an off-line measurement. There is one remaining subfunction that determines the combustion dynamics of the combustor and that needs to be determined by means of an experiment with the actively forced flame. With the method proposed, acoustic measurements on the steady, unperturbed flame and on the unsteady, actively perturbed flame in the DESIRE combustor are presented. The effect of pressure is investigated. The steady measurements are used to provide a finger print of the combustor with respect to the acoustic properties in interaction with combustion. In the unsteady measurements, the flame transfer function is reconstructed from the measured acoustic pressures. The measured FTFs are compared to FTFs which were calculated from a numerical experiment in Computation Fluid Dynamics (CFD) (see Kampen et al. (2003, 2004, 2008)). This is done at a range of power 100 to 300 kW and pressure 1 to 3 bars.

2. LITERATURE REVIEW

Numerous experimental studies have been performed in which the acoustic behaviour of a turbulent, premixed swirl flame is characterised. A categorisation of these experimental studies can be made on basis of whether the active or passive flame noise is studied. The active flame noise can only be measured when one of the inlet quantities of the flame is perturbed. Subsequently, the response of the flame in terms of the volume integrated heat release rate is monitored, either by acoustic measurements Paschereit et al. (2002) or by visual (laser, chemiluminescence etc.) techniques (see Kunze et al. (2004), Gentemann et al. (2004), Balachandran et al. (2005), Cheung et al. (2003)). The experiments discussed in literature are mostly performed at atmospheric pressure and at single burner rigs, see for example Lawn (1999). Examples of exceptions to this are the papers of Cheung et al. (2003) and Kunze et al. (2004). In the former paper, the FTF is determined at 15 bars (in the frequency range below 200 Hz), while the latter paper makes a comparison with transfer functions measured in an annular, multiburner experimental setup.

The passive noise produced by the flame can be measured in the same way as the active noise, only no exciter is required (see Cabot et al. (2004), Arana et al. (2002), Dawson and Fitzpatrick (2000), Krüger et al. (2001)). Consequently, passive noise experiments are more common at elevated pressures than active noise experiments. In some cases, the passive noise can be characterised by just installing dynamic pressure transducers in a combustor, which allows these measurements to be applied in existing combustors.

Yet another category of thermo-acoustic experiments are measurements on the self-excited system. In these measurements, the boundary conditions of the setup are modified until a self-excited oscillation is encountered (see Ng et al. (2005), Richards and Janus (1998), Hobson et al. (1999), Dawson and Fitzpatrick (2000), Elsari and Cummings (2003)). Subsequently, explanations are sought for the occurrence of the self-excited oscillation. Moreover, methods to remove the self-excited mode are often given. Sometimes, the limit-cycle behaviour of the self-excited instability is discussed (Lieuwen 2002).

As mentioned earlier, almost all actively perturbed experimental combustion setups seen in literature operate at atmospheric pressure. Nevertheless, the experience of most experimentalists is that the behaviour can significantly change when increasing the mean operating pressure of the rig. It is important to account for this effect, since the final application of most models would be to predict thermo-acoustic behaviour of combustion applications at elevated pressures (i.e. large scale gas turbines operate at a mean pressure around 20 bars). The realisation of an experimental combustion setup operating at elevated pressures has large consequences for the design, as well as for the way of operation due to extra safety procedures. Fortunately, the pressure level does not have to increase much to study the effect of the pressure on the thermo-acoustic behaviour of the flame. It is known that the largest influence of the pressure on combustion occurs in the lower pressure range (Warnatz et al. 1996).Therefore, the maximum operating pressure of the UT-DESIRE setup is 5 bars.

3. THE MECHANISM OF INTERACTION BETWEEN COMBUSTION DYNAMICS AND ACOUSTICS

Sound generation by turbulent flames originates from the fluctuating heat release in the flame. The description of this fluctuating heat release in turbulent flames is complicated due to the interaction of turbulence, mixing, combustion and noise. In a turbulent flame the instantaneous density, velocity, pressure, temperature and species concentrations are determined by the transport equations for mass, momentum, enthalpy and species and by the equation of state. Following the method presented by Sir James Lighthill (see Crighton et al. (1992)), the equations for mass and momentum can be combined to one equation in pressure and density. This equation relates instantaneous changes in pressure and density to fluctuations in velocity:

$$\frac{\partial^2 \rho}{\partial t^2} - \nabla^2 P = \nabla^2[(\rho \underline{u}\underline{u}) - \underline{\underline{\tau}}] \tag{1}$$

Defining the excess density:

$$\rho_e = (\rho - \rho_0) - \frac{P - P_0}{c_0^2} \tag{2}$$

The following well known pressure fluctuation propagation equation is obtained:

$$\frac{\partial}{\partial t}\left(\frac{1}{c_0^2}\frac{\partial P}{\partial t}\right) - \nabla^2 P = \nabla^2[(\rho \underline{u}\underline{u}) - \underline{\underline{\tau}}] - \frac{\partial^2 \rho_e}{\partial t^2} \tag{3}$$

It can be observed that eq (3) describes the propagation of pressure fluctuations at the wave speed c_0, at reference conditions. This equation contains source terms due to variations of the gradient of momentum transport and fluid stress. The most interesting source term here is the 3rd rhs, which represents the driving effect of density fluctuations, due to for example combustion. This source term can be related to the rate of heat transfer by means of the change of concentration of fuel and oxidizer and temperature. In fact this is quite a complicated expression (see Kok (2007)), but the combustion dynamics source term M can be simplified under a number of assumptions to:

$$M = \frac{\partial^2 \rho_e}{\partial t^2} \approx \frac{\gamma - 1}{c^2}\frac{\partial}{\partial t}(\dot{q}) \qquad \left[\frac{kg}{s^2 m^3}\right] \tag{4}$$

Here $\dot{q}$ is the local rate of thermal heat input to the gas per unit volume by combustion. In a gas turbine combustor it is however the total rate of thermal input by combustion that is observed and controlled, i.e. $\dot{q}$ integrated over the flame volume. This is denoted by $\dot{Q} = \int_{flame} \dot{q} dV$ and depends on the mass flows of fuel, $\dot{m}_f$, and of air, $\dot{m}_{air}$:

$$\dot{Q} = \dot{Q}\left(\dot{m}_f, \dot{m}_{air}\right) \qquad \left[\frac{kg.m^2}{s^3}\right] \tag{5}$$

Hence small fluctuations in the rate of combustion lead to a source term in eq (4) as given by the total derivative:

$$\frac{d\dot{Q}}{dt} = \left(\frac{\partial \dot{Q}\left(\dot{m}_f, \dot{m}_{air}\right)}{\partial \dot{m}_f}\right)_{\dot{m}_{air}} \frac{d\dot{m}_f}{dt} + \left(\frac{\partial \dot{Q}\left(\dot{m}_f, \dot{m}_{air}\right)}{\partial \dot{m}_{air}}\right)_{\dot{m}_f} \frac{d\dot{m}_{air}}{dt} \tag{6}$$

It can be observed that by eq (6) the source term in the pressure fluctuation equation, as determined by eqs (3,4), is coupled to the aerodynamic and chemical processes in the flame through the mass flows of fuel and air. The strength of this source term, is determined by its sensitivity for fluctuations in the mass flow rates of fuel and air. This sensitivity is given by the coefficients at the right hand side of eq. (6). It can be remarked that there is a linear dependence of the mean rate of heat release on the mean fuel mass flow rate. Assuming this linearity also extends to fluctuations with respect to the mean, the sensitivity coefficients in eq (6) can be represented by the transfer functions H_f and H_{air}. For practical application the transfer functions H_f and H_{air} in eq (6) are nondimensionalized, as shown in eq (7):

$$\frac{\frac{d\dot{Q}}{dt}}{\frac{\dot{Q}}{\dot{Q}}} = \frac{\dot{Q}'}{\dot{Q}} = H_f \frac{\dot{m}_f'}{\dot{m}_f} + H_{air} \frac{\dot{m}_{air}'}{\dot{m}_f} \qquad \left[\frac{1}{s}\right] \tag{7}$$

Here the fluctuation of a variable per time unit is denoted by $'$. It can be observed that the mass flow rate fluctuations per time unit of both fuel and air are nondimensionalized by the mean mass flow rate of fuel. This is done in view of the linear relation between the mean flow rate of fuel and the mean rate of heat release by combustion. This way the transfer functions will be less influenced by changes in power of the flame. The coefficients in eq (6) can now be related to the transfer functions in eq (7) by:

$$\left(\frac{\partial \dot{Q}\left(\dot{m}_f, \dot{m}_{air}\right)}{\partial \dot{m}_f}\right)_{\dot{m}_{air}} = \frac{\overline{\dot{Q}}}{\overline{\dot{m}_f}} H_f \tag{8}$$

$$\left(\frac{\partial \dot{Q}\left(\dot{m}_f, \dot{m}_{air}\right)}{\partial \dot{m}_{air}}\right)_{\dot{m}_{air}} = \frac{\overline{\dot{Q}}}{\overline{\dot{m}_f}} H_{air} \tag{9}$$

Depending on the validity of the assumption of linearity, the flame transfer functions H_f and H_{air} are applicable for small amplitudes of fluctuation and range of flame operation conditions. This assumption of linearity will experimentally be investigated in

Section 6. The effect of mean fuel mass flow rate (i.e. thermal power) and a combustion parameter like pressure will be explored subsequently.

4. GENERIC PROCEDURE FOR MEASURING FLAME TRANSFER FUNCTIONS

The flame transfer function can be determined by means of computation or experiment. In Van Kampen et al. (2007) efficient means to compute the flame transfer function on basis of CFD results were discussed. It is however important to measure the flame transfer function as well for specific cases for the validation of numerical results. To measure the flame transfer function is not trivial, as the instantaneous rate of heat release integrated over the combustor volume can not be measured directly. What can be measured easily and with high resolution, is the instantaneous pressure at a location. In this section a new generic method to measure the flame transfer function with the use of pressure transducers only, is presented. An overview of the different elements that play a role in the FTF reconstruction is shown in figure 1. During a FTF measurement, a fast valve in the fuel supply line is driven by an excitation signal V'_{exc}. This moves the valve with a displacement δ' per time unit, resulting in a fuel mass flow perturbation per time unit $\dot{m}'_f$ at the end of the fuel supply line. This eventually causes a heat release rate perturbation per time unit $\dot{Q}'$. Since according to eq (4) this perturbation is proportional to an acoustic sound source M, the perturbation can be measured by the pressure transducers in the combustion chamber. The FTF considered here, for the fuel mass flow rate oscillations, is defined here as

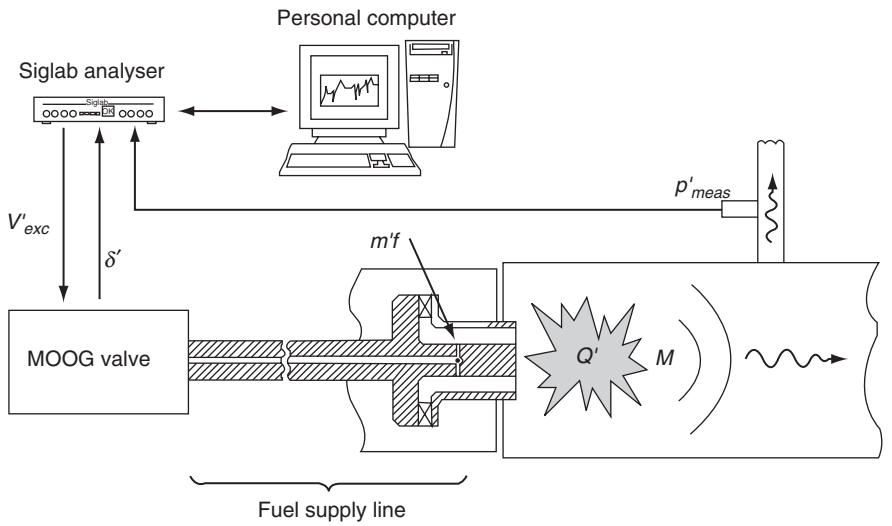

Figure 1: Flame Transfer Function measurement system lay out.

$$H_f = \frac{\overline{\dot{m}_f}}{\bar{\dot{Q}}} \frac{\dot{Q}'}{\dot{m}_f'} \qquad [-] \tag{10}$$

The direct effect of a fuel mass flow variation is a variation in the fuel to air equivalence ratio. It was shown in several papers that for premixed flames, equivalence ratio perturbations are the most likely cause for feedback to the flame (see Hobson et al. (2000), Hubbard and Dowling (2001), Lieuwen and Zin (1998), Cho and Lieuwen (2003)). Raman measurements have also been used (Weigand et al. 2005) in an unstable lean premixed methane swirl flame to show that indeed equivalence ratio perturbations are causing the instability. In lean combustion (equivalence ratio < 0.5) of natural gas, the air to fuel mass flow ratio is 30 or more. This implies that a perturbation in the fuel mass flow has the largest influence on the equivalence ratio. An advantage of perturbing the fuel mass flow is that the total mass flow of the reactant mixture is hardly perturbed. This way, the observed heat release rate fluctuation can assumed to be the result of the induced equivalence ratio perturbations. In this paper the effect of equivalence ratio fluctuations will be investigated by fluctuation of the fuel mass flow. The effect of variation of the mean equivalence ratio was not explored. The mean equivalence ratio was always set to 0.5. The relation between fuel mass flow (variation) and equivalence ratio (variation) is discussed in appendix 2.

The fuel mass flow Flame Transfer Function in eq. (10) can be factorized into six transfer functions, to allow its measurement:

$$H_f = \prod_{i=1}^{6} H_{fi} = \frac{\overline{\dot{m}_f}}{\bar{\dot{Q}}} \left\{ \frac{\dot{Q}'}{M} \cdot \frac{M}{p_{\underline{x}}'} \cdot \frac{p_{\underline{x}}'}{p_{\text{meas}}'} \cdot \frac{p_{\text{meas}}'}{\delta'} \cdot \frac{\delta'}{\dot{m}_f'} \right\} \quad [-] \tag{11}$$

This factorization was chosen with a view to the variables that can be measured, namely the MOOG valve piston displacement, the flame chemiluminescence intensity and the pressure as a function of time. The first factor when viewed from left to right in the flame transfer function at the right hand side is:

$$H_{f1} = \frac{\overline{\dot{m}_f}}{\bar{\dot{Q}}} \qquad \left[\frac{kg/s}{J/s}\right] = \left[\frac{s^2}{m^2}\right] \tag{12}$$

The second transfer function in equation (11) is obtained from thermodynamics as given in eq (4).

$$H_{f2} = \frac{\dot{Q}'}{M} = \frac{c_0^2}{\gamma - 1} V_{flame} \qquad \left[\frac{m^5}{s^2}\right] \tag{13}$$

In this factor is M the acoustic source driving the propagation of pressure fluctuations as determined in eqs (3,4), where c_0 and γ are determined at the adiabatic flame temperature. V_{flame} is the combustor volume.

The third transfer function in equation (11) describes the transfer function between the acoustic mass flow source represented by the flame, and the local pressure at a location $\underline{x}$ in the combustor:

$$H_{f3} = \frac{M}{p_{\underline{x}}'} \qquad \left[\frac{s}{m^2}\right] \tag{14}$$

This transfer function presents the "acoustic finger print" of the combustor and is characteristic for the acoustic behaviour of the combustion system. Ideally this transfer function will be provided by an acoustic model. The success of the method would however rely on the reliability of such an acoustic model. This condition is often difficult to satisfy in GT engines, especially at low frequencies. Therefore, a different approach is taken here. In this approach use is made of a combination of measured data and acoustic modeling to establish the acoustic finger print of the combustor. In steady operation every combustor has an autonomous source of sound due to broad spectrum flame oscillations. These are caused by interaction between spontaneous turbulence and combustion. This source is used here as a signal for M and the correlated induced sound field in the combustor to establish the transfer function in eq (14).

In this alternative approach, it is assumed that the autonomous flame source strength is a known function of the frequency. Measurements of open premixed flames show that the overall noise level strongly depends on burner size, engine power and flame temperature, but these factors have only a small effect on the spectral shape (Mahan et al. 1991). Additionally, parametric studies of acoustic radiation from premixed natural gas-fuelled turbulent flames show that, for a fixed burner diameter, the acoustic spectrum of the flame has a nearly universal shape, whose total power density is a function of equivalence ratio and flow velocity (Rajaram and Lieuwen 1998).

On basis of the above, the spectral shape of the acoustic source due to autonomous combustion fluctuations is investigated. This shape can be determined from the time series of measurements of the chemiluminescence of a flame in the wave length of light emitted by the excited CH* radical. The concentration of excited CH* is linearly proportional to the rate of heat release in the flame. Through equation (4) it follows then that the spectrum of the fluctuations of CH* is representative for the spectrum of the acoustic source, because:

$$M \sim \frac{\partial}{\partial t}(\dot{q}) \tag{15}$$

Now use can be made of the property of a Fourier transform F{ } that:

$$F\left\{\frac{\partial}{\partial t}(\dot{q})\right\} = i\omega F\{\dot{q}\} = i\omega\dot{q}(\omega) \tag{16}$$

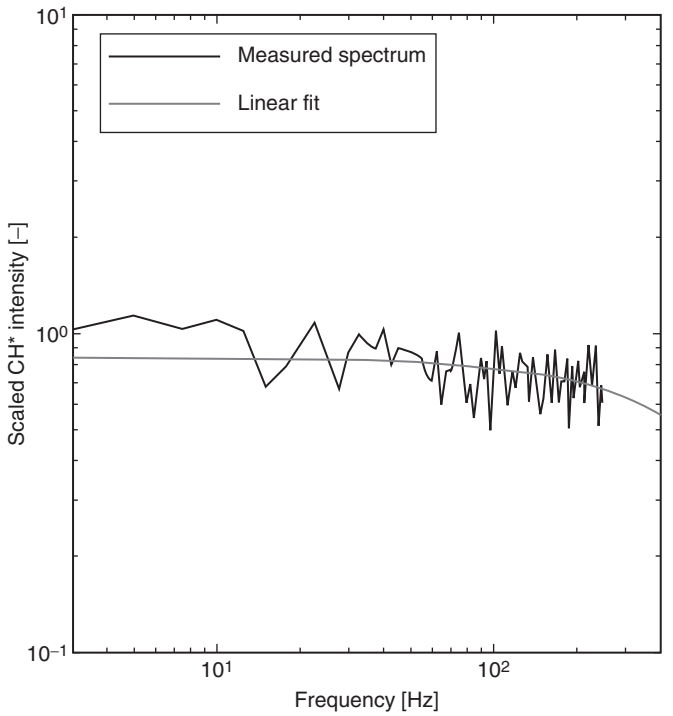

Figure 2: Measured spectrum of the CH* intensity of an autonomously fluctuating turbulent flame in the UT-DESIRE setup.

As an example, the measured spectrum of the CH* intensity of an autonomously fluctuating turbulent flame in the UT-DESIRE setup (as to be described in section 5) is shown in figure 2. A smooth spectrum is observed, of which the shape is approximately flat at low frequencies, and slightly rolls off at higher frequencies. From the spectrum of the fluctuations of the CH* intensity, a spectral shape for the autonomous source $M_{auto}(\omega)$ is extracted by fitting the spectrum with a linear function (see figure 2). The absolute level is however still unknown, as the chemiluminesce does not give information on absolute concentrations of CH*, only relative to a reference level.

Next to be determined is the spectral shape of the pressure oscillations $p'_x(\omega)$ per time unit. Here also use is made of the property of Fourier transforms $F\{\}$:

$$F\left\{\frac{\partial}{\partial t}\left(p_x(t)\right)\right\} = i\omega F\{p_x(t)\} = i\omega p_x(\omega) \tag{17}$$

With a view to our proposed measurements, for $\underline{x}$ would have to be chosen the location of the pressure transducer in the test rig. In that case use can be made of the measured auto spectrum $p_{auto}(\omega)$ at steady unperturbed conditions in the combustor,

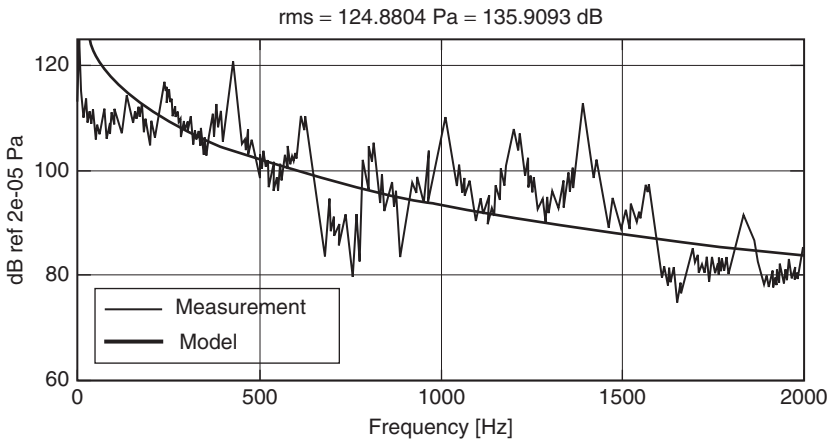

Figure 3: Measured pressure transducer autospectrum of an autonomously fluctuating turbulent flame in the UT-DESIRE setup.

that is explored. As an example the measured autospectrum at pressure transducer location *P*2 of an autonomously fluctuating turbulent flame in the UT-DESIRE setup (as to be described in section 5) is shown in figure 3. The sound pressure level is observed to be at a maximum at low frequencies, approximately 140 dB. With increasing frequency the sound level decreases, with exception of a few eigenfrequency points, smoothly to 85 dB at 2,000 Hz. The measured data show some eigenfrequencies, for example 400, 600, 800, 1000 Hz. Here the sound pressure level rises with about 10 dB. The fitted line presents predictions by a combustion dynamics model, that does not take into account the finite length of the combustor (see De Jager and Kok, (2006)). Clearly the acoustic finger print of the combustion system is made visible here.

The ratio between the level of the acoustic source and the pressure fluctuation at location x is still to be determined now. This can be done with the use of an acoustic model. Note that this model usually gives a bad representation of the shape of the flame source spectrum, however it is only used here to determine the ratio of the spectra $M(\omega)$ and $p'_x(\omega)$.

The method sketched above gives as an approximation for the transfer function:

$$H_{f3} = \frac{M}{p_x(\omega)'} \cong \frac{i\omega\dot{q}(\omega)}{i\omega \mathrm{p_x}(\omega)} = \frac{\dot{q}(\omega)}{\mathrm{p_x}(\omega)} \tag{18}$$

And in approximation:

$$H_{f3} = \frac{\dot{q}(\omega)}{\mathrm{p_x}(\omega)} \approx \frac{\dot{q}_{auto}(\omega)}{p_{auto}(\omega)} \exp\left(i\left(k\omega t + \varphi_0\right)\right) \tag{19}$$

While the amplitude of the transfer function H_{f3} is determined now, the phase information k and φ_0 remain unspecified. The phase information is related to the fact

that the pressure is recorded not at the combustion source location but at some distance at a wall location. In principle this can be derived from the acoustic model. This is however not necessary when it is taken into account that due to the high combustion temperatures the speed of sound is approximately 1000 m/s, and the pressure transducer that records $p_{\text{auto}}(\omega)$ is at a distance of the order of 0.1 m from the flame sound source. In that case, in the frequency range considered here: 50–500 Hz, the phase shift can be neglected and the phase factor in eq (19) becomes unity.

Finally the following expression is obtained for the transfer function H_{f3} (the acoustic finger print) from a combination of measured data on the flame source, the pressure autospectrum and the acoustic system model:

$$H_{f3} = \frac{M}{p(\underline{x})'} \approx \frac{\dot{q}_{auto}(\omega)}{p_{auto}(\omega)} \qquad \left[\frac{s}{m^2}\right] \tag{20}$$

The 4th transfer function H_{f4} is equal to unity, when the location of the pressure transducer for the autonomous noise measurements is taken equal to the location of the pressure transducer for the transfer function measurements.

The 6th transfer function is defined as:

$$H_{f6} = \frac{\delta'(\omega)}{\dot{m}_f'(\omega)} \qquad \left[\frac{m.s}{kg}\right] \tag{21}$$

This transfer function describes the transmission of a signal of the excitation instrument (like a siren, a loudspeaker or as taken here a MOOG valve) to the fuel mass flow. As this transfer function depends very much on the properties of the excitation instrument and the fuel line transmission, it is best to retrieve it from experimental data. This data needs to be available for the entire range of power and pressure of the investigated points of operation of the combustor. To retrieve these data, separate fuel supply line experiments were performed. These (cold) experiments are performed on a model setup of the fuel supply line. They are intended to measure the relationship between a perturbation per time unit in the fuel flow at the upstream end of the supply line by a displacement of the MOOG valve piston, and the final fuel mass flow perturbation per time unit at the injection location. The applied method and results are described in detail in section 5.2.

Now that the transfer functions H_{f1}, H_{f2}, H_{f3}, H_{f4} and H_{f6} have been determined, the total transfer function H_f can be determined by closing the data with H_{f5}. This is the only data that requires a dynamic combustion measurement, and that contains the dynamic properties of the acousto-combustion system. Hence H_{f5} is directly measured in the experiment:

$$H_{f5} = \frac{p'_{\text{meas}}(\omega)}{\delta'(\omega)} \qquad \left[\frac{kg}{m^2 s^2}\right] \tag{22}$$

Since the ratio of the cross-spectrum and the auto-spectrum of the two signals is taken to determine the transfer function, uncorrelated noise in the measured pressure signal does not influence the transfer (Herlufsen 1984). Because the valve displacement signal is noise free, the measured transfer only includes the active noise of the flame.

$$H_f = \prod_{i=1}^{6} H_{fi} = \frac{\overline{\dot{m}_f}}{\overline{\dot{Q}}} \left\{ \frac{\dot{Q}'}{M} \cdot \frac{M'}{p_{\underline{x}}'} \cdot \frac{p_{\underline{x}}'}{p'_{\text{meas}}} \cdot \frac{p'_{\text{meas}}}{\delta'} \cdot \frac{\delta'}{\dot{m}_f'} \right\} \qquad [-] \qquad (23)$$

Data obtained for the flame transfer function H_f, following the above method, are described in section 6. Prior to this, in Section 5 will be described the combustor test rig that was used for the experiment and the measurement procedure.

5. EXPERIMENTAL SET UP AND MEASUREMENT PROCEDURE

In this section the experimental preparation and validation of the tools presented in the previous sections is discussed. First, the layout of the UT-DESIRE setup is presented, along with a description of its measurement equipment. Subsequently the method and typical result for the transfer function H_{f6} (the correlation between MOOG valve dynamics and fuel mass flow dynamics) is presented.

5.1. Combustor test rig

A cross-section of the UT-DESIRE combustor, showing its main components, is illustrated in figure 4. The combustor consists of two square tubes. The inner square tube forms the liner and the outer square tube is the pressure vessel. Between the tubes the cooling air flow is forced. The burner opens into the inner square tube with cross-section 0.15×0.15 m^2 in which the combustion process of the air/natural gas mixture

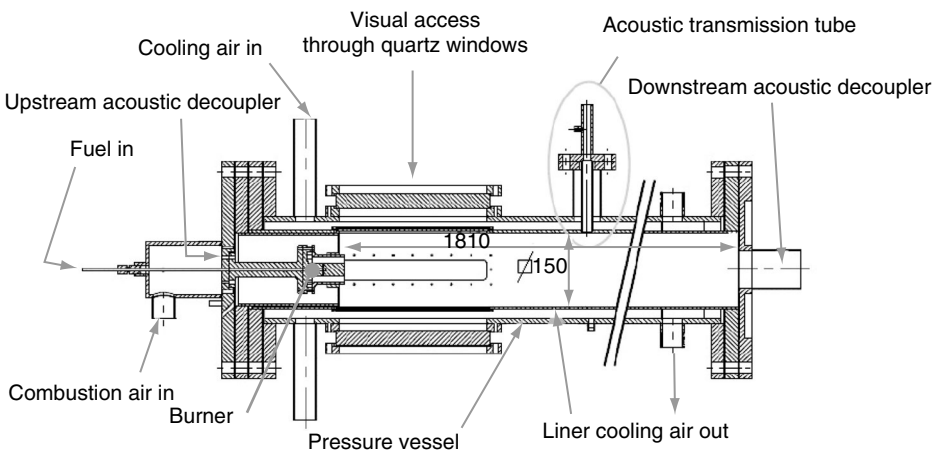

Figure 4: Cross-section of the UT-DESIRE combustor.

takes place. The combustion process can be observed optically with a 1 kHz high speed camera (Laser Induced Fluorescence and natural light emission by chemiluminescence) through quartz glass windows that are mounted on 3 sides in the liner and pressure vessel. The burner is of the radial swirler type (with a swirl number of about 0.7). It is designed to operate under lean conditions at a nominal power of 100 kW/bar, burning Dutch natural gas. The burner is supplied with air preheated to 300 C from a plenum. The plenum is separated from the hot gasses in the combustion chamber by a flame shield. The air flow in the plenum cools the flame shield. Four fuel nozzles in the central hub of the burner inject natural gas in the swirling air flow. At the burner exit, a technically premixed lean combustible mixture flows into the combustor. At the start of a test session, the combustible mixture is ignited by a spark plug, located in the corner of the combustion chamber.

The UT Desire test rig has a very stable 10 bar air supply by means of a screw compressor. Connected to this compressor are two Bronkhorst mass flow controller valves to adjust the combustion air and cooling air flow. The combustion air flow is heated by a 120 kW thermostat controlled electric heater prior to its entrance in the combustor. A small screw compressor supplies natural gas at 9 bar to the test rig. This fuel flow is also controlled by a Bronkhorst mass flow controller valve. Downstream the Bronkhorst valve the fuel flow is led via a MOOG valve (that can oscillate the flow) to the burner in the test rig.

The preheated combustion air is supplied to the plenum through 12 holes with a diameter of 7 mm. These holes act as an acoustic decoupler, due to the high velocity, large area contraction and high pressure drop. A similar acoustic decoupler is constructed downstream the combustor (see figure 4). Here, a single contraction with a diameter of 75 mm provides an acoustically hard end condition. As a result of the upstream and downstream acoustic decouplers, the system beyond the decouplers does not have to be accounted for in the acoustic modelling.

All operating points considered in this paper have an air factor of 1.8 with an air preheating temperature of 300 C. Consequently, the pressure and the power fully define the inlet boundary conditions of the combustor. The operating points that are considered in this paper are indicated with a code, for instance 125.15. In this code, the first number indicated the power in kW and the second number indicates the pressure in decibar. The acoustic pressure is measured at several locations in the main combustor, using a so-called acoustic transmission tube. The measurement technique, as well as the post-processing applied to the acoustic measurements to separate the flow noise from the flame source, are described in appendix 1.

5.2. Characterisation of the fuel line

For the reconstruction of the FTF from the measurements, the fluctuating fuel mass flow at the fuel nozzle as a function of the MOOG valve needle displacement per time unit must be determined. The MOOG valve is located at approximately 1 metre upstream of the fuel supply nozzles, and connected by the fuel supply line. Due to acoustic effects in the fuel supply line, the mass flow perturbation at the MOOG valve can be shifted in amplitude and time with respect to the mass flow perturbation at the

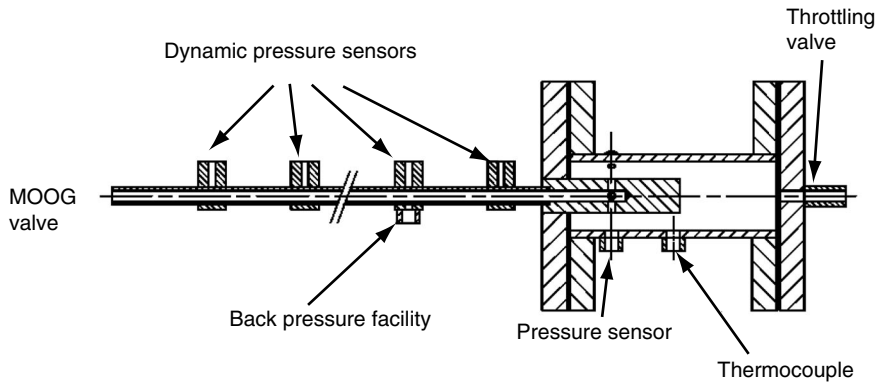

Figure 5: Experimental model of the fuel supply at 1:1 scale.

fuel nozzles. This relation between MOOG valve needle displacement per time unit and fuel mass flow perturbation per time unit is described by the transfer function H_{f6}:

$$H_{f6} = \frac{\delta'(\omega)}{\dot{m}_f{}'(\omega)} \qquad \left[\frac{m.s}{kg}\right] \tag{24}$$

Due to lack of access and possible disturbance of the flow, it is not possible to measure the fluctuating fuel mass flow directly at the nozzles of the DESIRE setup during a FTF measurement. For this reason a 1:1 scale experimental model of the fuel supply (see figure 5) is made (see also Kleinlugtenbelt (2005)). It can be seen that only the annular passage of the burner is included in the experimental model. Simulated experiments with the acoustic network model showed that the combustion chamber, downstream the annular burner passage, hardly influences the acoustic fluctuations at the fuel nozzles (see Kleinlugtenbelt (2005)). The high velocities and pressure drop prevent acoustic waves to significantly propagate from the combustor into the fuel supply line. In the real-scale model, the mass flow perturbation at the fuel nozzles has been reconstructed from the pressure fluctuation measured by a pressure transducer in the annular passage. The relationship between pressure fluctuations and mass flow fluctuations at the fuel nozzles is explained with the help of a schematic view of the annular passage in which the fuel nozzles exit (see figure 6). A fluctuating mass flow M_{0f} enters the annular passage. The pressure perturbation p_0 in the annular passage is measured with a Kulite pressure transducer. The annular passage has a volume V and the flow exits the annular passage via a nozzle. The flow in the nozzle is (near) choking, so an acoustic reflection coefficient of 1 is assumed at this exit.

The dimensions of the annular passage are small compared to the acoustic wavelengths in the considered frequency range. This means that a quasi-steady acoustic approach can be used to transform the measured pressure to the velocity perturbation at the fuel nozzles. Integrating the mass conservation equation over the volume of the annular passage gives:

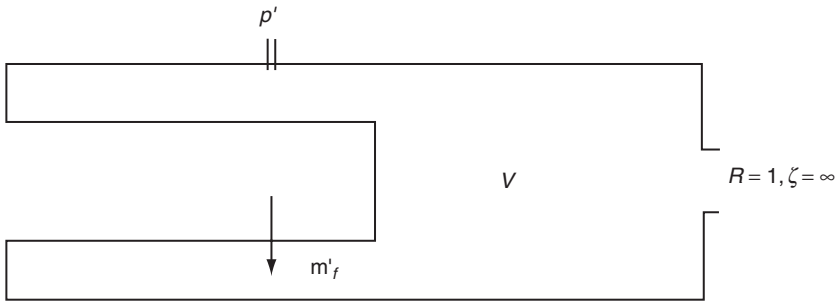

Figure 6: Schematic acoustic situation of the annular passage in which the fuel nozzles exit.

$$\int_V \left(\frac{\partial \rho}{\partial t} + \nabla.(\rho \underline{u}) \right) dV \approx V \frac{d\rho}{dt} + \int_V \nabla.(\rho \underline{u}) dV = 0 \tag{25}$$

where the quasi-steady assumption is used that the density does not depend on the location (i.e. no standing waves). Applying the Gauss theorem yields:

$$V \frac{d\rho}{dt} + \int_S (\rho \underline{u}.\underline{n}) dS = 0 \tag{26}$$

The cross sectional areas S_{in} and S_{out} are denoted as the total area of the four fuel nozzles and the area of the exit of the passage, respectively. Similarly, u_{in} and u_{out} are the velocity perpendicular to the exit cross sectional area of the fuel nozzles and of the burner passage, respectively. Equation (26) above can now be written as:

$$V \frac{d\rho}{dt} + \rho \left(u_{out} S_{out} - u_{in} S_{in} \right) = 0 \tag{27}$$

Linearising this equation and assuming a harmonic time dependence gives:

$$Vi\omega \Delta\rho - \Delta u_{in} \rho S_{in} = 0 \tag{28}$$

The velocity perturbation at the outlet completely disappears since an acoustic reflection coefficient of 1 was assumed. Using the isentropic relationship between the acoustic pressure and density ($\Delta P = c_0^2 \Delta\rho$), this can be rewritten as:

$$Vi\omega \frac{\Delta P}{c_0^2} - \Delta u_{in} \rho S_{in} = 0 \tag{29}$$

Hence, the fuel mass flow fluctuation per time unit summed over all four fuel nozzles can be written as:

$$m_f' = \frac{\Delta u_{in}}{\Delta t}\rho S_{in} = Vi\omega \frac{\Delta P}{\Delta t}\frac{1}{c_0^2} \qquad \left[\frac{kg}{s^2}\right] \tag{30}$$

With this equation, the measured pressure as a function of time can be used to determine the fuel mass flow perturbation per time unit at the fuel nozzle exit by numerical differentiation. Using a pressure transducer appears to yield more reliable data than measuring the velocity fluctuation downstream the nozzles with a hot-wire sensor. When a hot-wire would be used, a few assumptions would have to be made: a constant velocity profile in radial direction at any moment within a period of oscillation, rotational symmetry and an incompressible flow. These assumptions can break down. Firstly, the conventional steady flow Nusselt number correlations for heat exchange of the hot-wire are not applicable to pulsated flows, as the boundary layer is transient. Secondly, the velocity profile can change as a function of the frequency. Both effects can influence the velocity measured by the hot-wire. Therefore the mass flow perturbation reconstructed from the measured unsteady pressure is more reliable.

The transfer function H_{f6}, between the displacement per time unit of the MOOG valve piston and the fuel mass flow perturbation per time unit at the fuel nozzles, can now be evaluated with the use of eq. (30):

$$H_{f6} = \frac{\delta'(\omega)}{\dot{m}_f'(\omega)} = \frac{\frac{\triangle\delta}{\triangle t}}{Vi\omega \frac{\triangle P}{\triangle t}\frac{1}{c_0^2}} \qquad \left[\frac{m.s}{kg}\right] \tag{31}$$

In eq. (31) it can be observed that both the MOOG valve displacement and the pressure signal need to be differentiated numerically with respect to time. As in eq. (31) just the ratio of both signals per unit time is needed, this differentiation can be avoided by multiplying the ratio by Δt. It follows then that the transfer function H_{f6} can be evaluated directly on basis of the measured correlation between the displacement of the MOOG valve piston and the pressure perturbation at the fuel nozzle exit:

$$H_{f6} = \frac{\delta'(\omega)}{\dot{m}_f'(\omega)} = \frac{\triangle\delta}{Vi\omega \frac{1}{c_0^2}\triangle P} \qquad \left[\frac{m.s}{kg}\right] \tag{32}$$

An example of the transfer function H_{f6} between the displacement per time unit of the MOOG valve piston and the fuel mass flow perturbation per time unit at the fuel nozzles, obtained at operating point 15.7 is shown in figure 7. The transfer is determined at discrete frequencies by using a sinusoidal excitation. Although the frequency resolution with this type of excitation is less than with, for example, a sinus sweep excitation, the coherence is perfect, even for lower frequencies. The phase shift that is noticed between the MOOG piston displacement per time unit and the mass flow fluctuation at the fuel nozzle per time unit is almost perfectly linear. This shows that

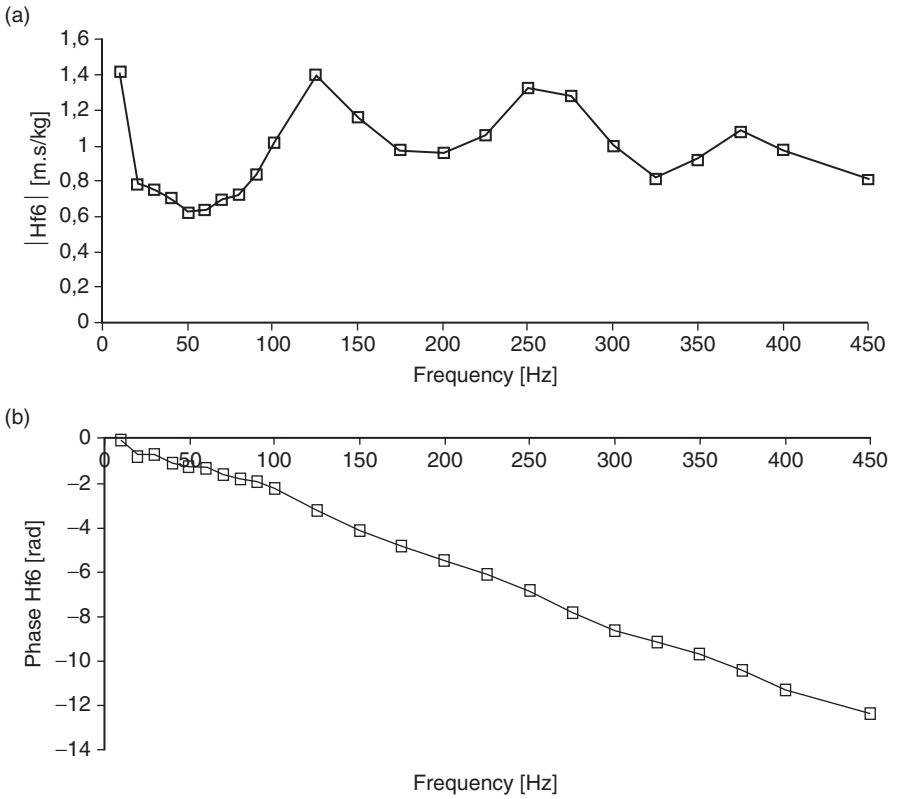

Figure 7: Transfer function H_{f6} between the displacement per time unit of the MOOG valve piston and the reconstructed mass flow perturbation per time unit at the fuel nozzles obtained at operating point 15.7.

there is a constant time delay between the two locations. Using the length of the fuel supply line and the sum of the speed of sound and the convection speed, the time delay should be 4.2 ms. The time delay derived from the measured phase is 4.4 ms. This corresponds well with the calculated delay.

5.3. Method of excitation of Equivalence Ratio Oscillations

To perturb the fuel supply of the flame, a D633-7320 MOOG control valve is used. In the MOOG valve, the fuel flow into the fuel line is perturbed by oscillating a free piston, driven by an electric coil in a magnetic field. The actual position of the piston is measured by a Linear Variable Differential Transformer.

In the FTF measurements, it is attempted to have a constant amplitude of perturbation of the fuel mass flow at all considered frequencies. The displacement amplitude of the MOOG piston measured at constant driving voltage and as a function of frequency is shown in figure 8. It can be observed that the amplitude decreases with

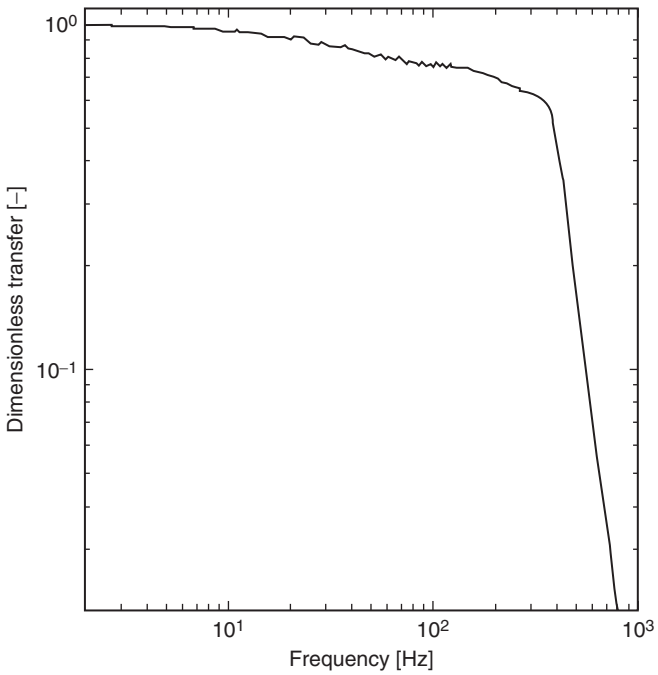

Figure 8: Displacement amplitude of the MOOG valve piston measured at constant driving voltage and as a function of frequency.

frequency. The valve has a cut-off frequency of 420 Hz. Above this frequency, the level of excitation decreases rapidly. Additionally, the fuel supply line transfer function (figure 7) shows to the MOOG valve piston oscillation a frequency dependent response of the velocity oscillation at the fuel nozzles. Both effects imply that the MOOG excitation voltage has to be frequency dependent to achieve a constant level of velocity perturbation at the fuel nozzles.

The level of excitation that can be reached is limited though: it is bounded by the maximum displacement of the MOOG piston. When a constant amplitude of 5% of the mean fuel mass flow is desired, the required excitation amplitude of the MOOG valve is shown in figure 9 for a power of 125 and of 150 kW, both at 1.5 bars. In this figure, an additional line is displayed, showing the excitation at which the maximum piston displacement is reached. This is a boundary for the maximum excitation that can be achieved. It can be observed that the necessary excitation amplitude varies slightly with frequency in the range 70–400 Hz. At 60 Hz a very high excitation amplitude, at maximum piston displacement, is necessary due to the acoustics of the fuel line. At frequencies above 400 Hz the necessary excitation level becomes very high due to the cut off of the MOOG valve. At frequencies below 50 Hz the necessary excitation amplitude decreases rapidly.

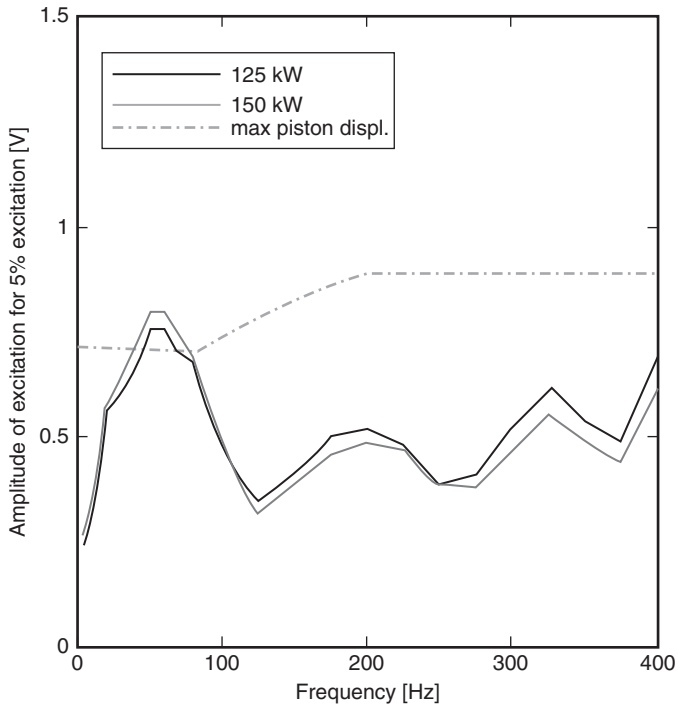

Figure 9: Required excitation amplitude of the MOOG valve for a constant amplitude of 5% of the mean fuel mass flow for a power of 125 and of 150 kW, both at 1.5 bars.

To demonstrate that an excitation of 5% indeed is in the (approximate) linear regime of the fuel supply line, the amplitudes of the reconstructed relative velocity fluctuation and the piston displacement are plotted as a function of the excitation level in Volts in figure 10. Here the MOOG valve is driven with a frequency of 200 Hz for operating point 15.7. In the figure, the piston displacement is normalised to a value of 2.5% at the lowest excitation. It can be seen that non-linear behaviour commences quite soon. A velocity fluctuation of 5% is considered as the maximum level at which the fuel supply line amplitude correlates linearly with the driving voltage (at 200 Hz, taken to be a representative frequency).

Using the procedure described above, the transfer function H_{f6} is measured at the operating points at which the FTF is to be determined. The measured transfers are used during the unsteady measurement to calculate the fuel mass flow perturbation per unit of time from the known displacement per time unit of the MOOG valve.

The flame is excited by the MOOG valve at several operating points. Use is made of the Virtual Swept-Sine (VSS) option of the Siglab spectral analyser. In this method, a sine wave is used as system excitation and discrete frequencies of the sine wave are stepped through the frequency range of interest. This excitation method gives the

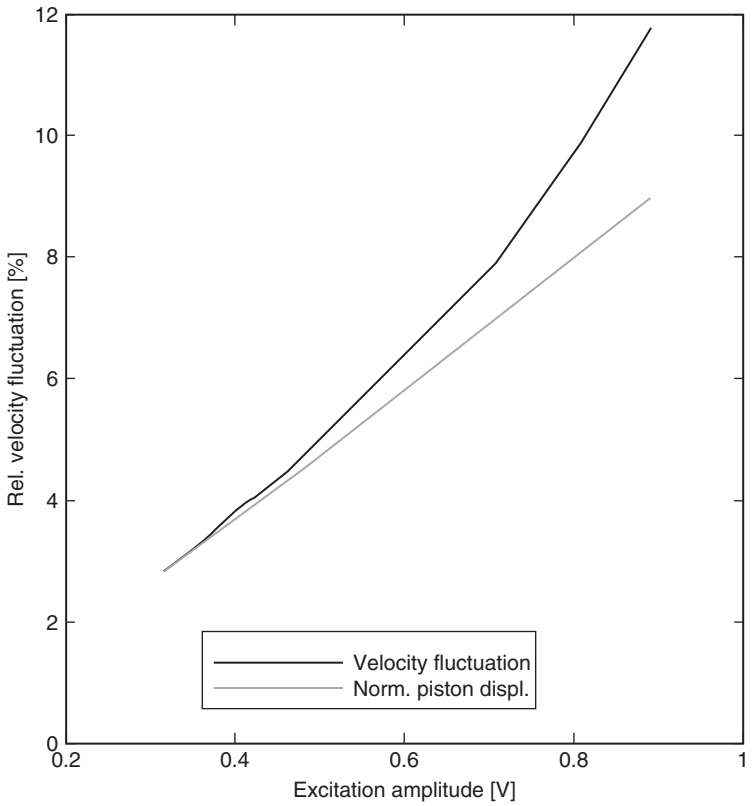

Figure 10: Amplitudes of the reconstructed relative velocity fluctuation and the piston displacement plotted as a function of the excitation level in Volts.

highest measurement accuracy. Linearity of the measured transfers is checked by comparing measured transfer functions obtained with different levels of excitation at operating point 125.15. This is done for excitation levels of 2.5%, 5%, 7.5% and 10% of the mean fuel mass flow. At these levels, the transfer function $H_{f5} = \frac{p'_{meas}}{\delta'}$, between the measured acoustic pressure and the MOOG displacement is measured. Hence, this transfer contains the fuel supply line transfer, the transfer between the fuel mass flow perturbation at the nozzles and the heat release rate response, and the transfer from this response to the measured acoustic pressure. A total of 84 frequencies are used, almost equally distributed in the range between 5 and 400 Hz. Figure 11 shows the amplitude and phase of the transfers. For a linearly behaving system, all transfer functions should be identical. For the phase, this is the case. The amplitude, however, shows deviations up to 25% in the high frequency region. The deviation from linearity at the higher frequencies can be mainly attributed to the non-linear behaviour of the fuel supply line

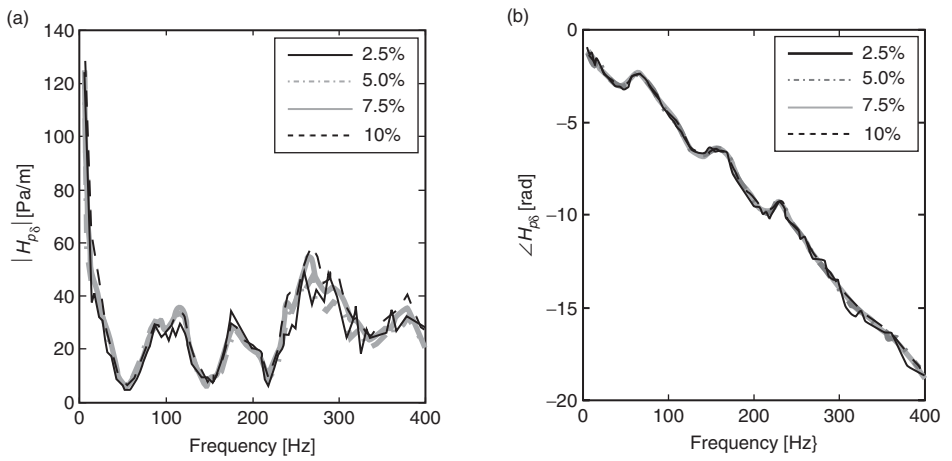

Figure 11: Transfer function $H_{f5} = p'_{meas}/\delta'$, between the measured acoustic pressure fluctuation and the MOOG displacement per time unit at excitation levels of 2.5%, 5%, 7.5% and 10% of the mean fuel mass flow: (a) Amplitude and (b) Phase.

(see section 5.2). This non-linear behaviour can lead to a considerably higher fuel mass flow perturbation than expected from linear assumptions (see van kampen (2006)). To remain in the linear regime *and* have enough excitation, 5% excitation is a good compromise and is used for the FTF measurements that will be presented in the remainder of this paper.

6. INTERACTION BETWEEN COMBUSTION DYNAMICS AND EQUIVALENCE RATIO FLUCTUATIONS: MEASURED FLAME TRANSFER FUNCTIONS

6.1. Behavior at atmospheric pressure

Firstly, the phase of the measured FTF according to equation 11 is considered. In this equation, the dominant phases determining the total phase shift of the FTF are the phases of H_{f5} and H_{f6}. The measured phase of the FTF is plotted in figure 12(a) and (b) for cases 150.15 and 125.15, respectively. In the figures, the measured phase is compared with the phase obtained from numerical simulations. These numerically obtained transfer functions have been obtained from a numerical experiment in CFD, i.e. the numerical flame is excited by an impulse excitation in a transient simulation. Subsequently, a spectral analysis of the time series yields the FTF. For details on these calculations, see Van Kampen (2006) and Van Kampen et al. (2004, 2008).

The agreement between the measurements and the simulations is good, for both the individual cases and the trends between the cases. Both the measurements and the simulations show an approximately linear frequency dependence of the phase. This indicates that a constant (convective) time delay exists between the excitation and the

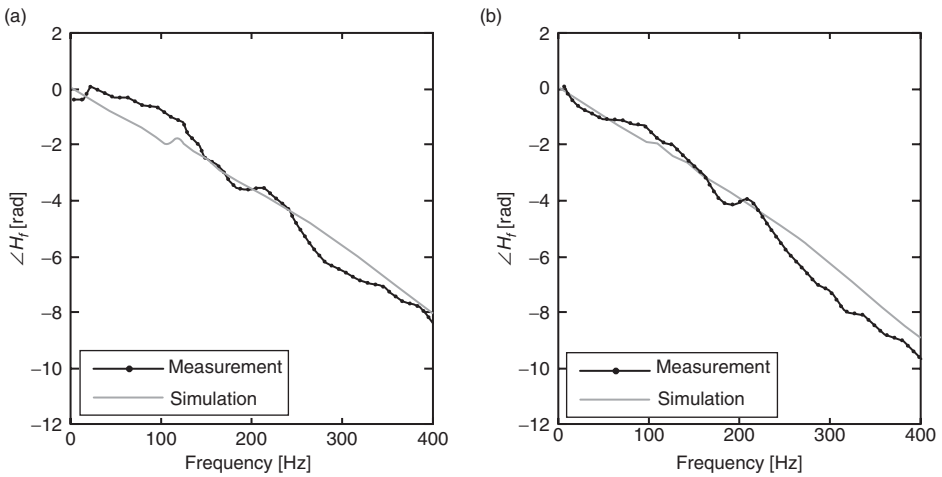

Figure 12: Measured phase of the Flame Transfer Function for cases 150.15 (a) and 125.15 (b).

response. The time delays can be extracted from a linear fit of the phase lines. For the measurements, this yields a time delay of 3.8 ms for case 125.15 and 3.3 ms for case 150.15. The decrease of the time delay with power can be explained from the higher convection velocities at case 150.15. Compared to case 125.15, case 150.15 has 20% higher velocities. Nevertheless, the measurements show only an 8% decrease of the time delay when increasing the power from 125 to 150 kW. This trend is also observed in the simulations: time delays of 3.3 ms (125.15) and 3.0 ms (150.15) can be derived from a linear fit of the phase lines. The decrease of time delay here is 10%. The explanation for this lower-than-expected decrease of the time delays is the location of the flame. Simulations show that the 125.15 flame is located closer to the burner exit than the 150.15 flame. This decreases the traveling distance (and time) from the excitation location to the flame location, which counteracts the increasing time delay due to the decreasing volume flow.

The amplitudes of the measured transfer functions are shown in figures 13 (a) and (b), respectively. The transfer shows a low-pass filter behaviour. The measured FTFs are normalised by the average value of the amplitudes between 5 and 20 Hz. The dimensionless transfer function is indicated as $H_f = \frac{\overline{\dot{m}_f}}{\bar{\dot{Q}}} \frac{\dot{Q}'}{\dot{m}_f'}$. A deviation of approximately 10% is noticed between the unnormalised quasi-steady values of the simulations and the measurements.

The experimentally obtained transfer functions show behaviour similar to those obtained from the simulations. A remarkable agreement is seen for case 150.15 (figure 13(a)). Just before the spectrum cuts off, the experiments and the simulations agree very well. The spectrum cuts off purely due to the volume integration of the heat release rate

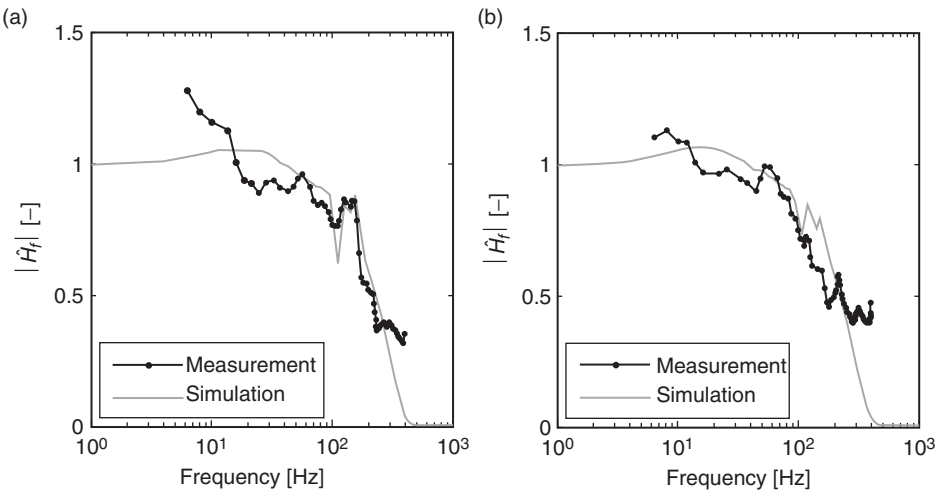

Figure 13: Measured amplitude of the Flame Transfer Function for cases 150.15 (a) and 125.15 (b).

over the flame zone. This can be understood by the fact that the wavelength λ of the equivalence ratio excitation is based on the convective velocity rather than the speed of sound, i.e.:

$$\lambda_{eq} = \frac{u_{gas}}{f_{exc}}. \tag{33}$$

Still, volume integrating the acoustic source is justified from an acoustical point of view because the flame length is much smaller than the acoustic wavelength. At the frequency:

$$f_{exc} = \frac{u_{gas}}{\lambda_{eq}} = \frac{u_{gas}}{L_{flame}}, \tag{34}$$

where the period of the fluctuating heat release rate equals the flame residence time, the integrated heat release rate fluctuation is zero (a similar result was obtained by Gentemann et al. (2004)). Hence at this excitation frequency the amplitude of the flame transfer function will vanish. Indeed in figure 13 a severe dip in the amplitude can be observed at 100 Hz. At twice this frequency, at which half of a wavelength fits in the flame, the FTF starts to fall off. At this and higher frequencies the local heat release fluctuations partially compensate each other, when integrated over the flame volume and the sensitivity to equivalence ratio waves is very much reduced. The low-pass behaviour is thus caused by the flame length being significantly larger than the equivalence ratio oscillation wave length.

Apart from the low-pass behaviour of the FTFs, the FTF of case 150.15 shows a peak at the cut-off frequency. A CFD analysis in which particles are tracked in the central and outer recirculation zone shows that it is likely that this peak is caused by the outer recirculation zone. When the period is equal to the time that a particle needs to complete a full circulation in the outer recirculation zone, an interaction effect of the heat released in the previous period with the currently released heat occurs. This interaction shows up as a peak in the amplitude spectrum. Since the outer recirculation zone is about half the size of the flame domain, the time for a particle to complete the full outer recirculation zone is approximately twice the flame residence time. Therefore, the frequency at which a full wavelength fits in the outer recirculation zone corresponds to the frequency at which half an equivalence ratio wavelength fits in the flame. Consequently, in the present combustor design the peak always occurs at approximately the same frequency as the cut-off frequency.

6.2. Behavior at elevated pressure

In the previous section two cases both at operating pressure 1.5 bars but different thermal power and gas velocities were compared. In this section, several operating points at elevated pressures are considered, while keeping the thermal power to pressure ratio constant at either 83 or 100 kW/bar. The latter power to pressure ratio is identical to that of operating point 150.15, and hence the gas velocities and convection velocities are identical too. This way the effect of a pressure rise can be investigated, while keeping the fluid dynamic processes unchanged. The effect of pressure at a lower power to pressure ratio is investigated at power to pressure ratio 83.

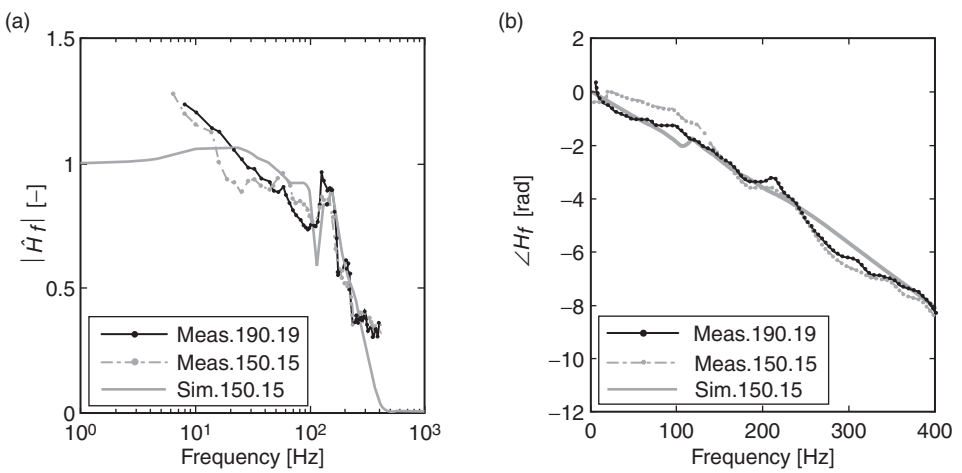

Figure 14: Amplitude and phase of the Flame Transfer Function at operating points 190.19 and 150.15 (power to pressure ratio 100 kW/bar): (a) Amplitude and (b) Phase.

Power to pressure ratio 100 kW/bar

The first discussed operating point 190.19 has a power to pressure ratio of 100 at an operating pressure of 1.9 bars. The FTF at operating point 190.19, reconstructed from the measured transfer between the MOOG piston displacement and the acoustic pressure in the combustor, is compared to the modelled transfer function in figure 14. In this figure, the measured FTF at operating point 150.15 (same velocities) is depicted as well.

Just as in the simulations, the measured transfer function at operating point 190.19 shows very little difference with the FTF at operating point 150.15. Again, the two peaks just before the amplitude spectrum cut off are noticed in both the measured and the modelled FTF. The cut-off frequency is also predicted well by the model, indicating a good prediction of the flame length.

The time delay that can be extracted from the phase plot is similar to the time delay of 150.15, i.e. 3.3 ms. Since the velocity fields are similar for both cases, this equal time delay indicates that the flame location does not change much when maintaining a constant ratio of power to pressure. The simulation also predicts an almost equal time delay.

Power to pressure ratio 83 kW/bar

Now the results will be discussed of operating points at power to pressure ratio 83 and pressures 1.5, 2.3 and 3 bars.

The measured FTF at operating points 192.23 and 250.30 is compared to the transfer at operating point 125.15. While the simulations show few differences between the compared cases, the measurements show an effect of the pressure on the FTF, as can be noticed from figure 15.

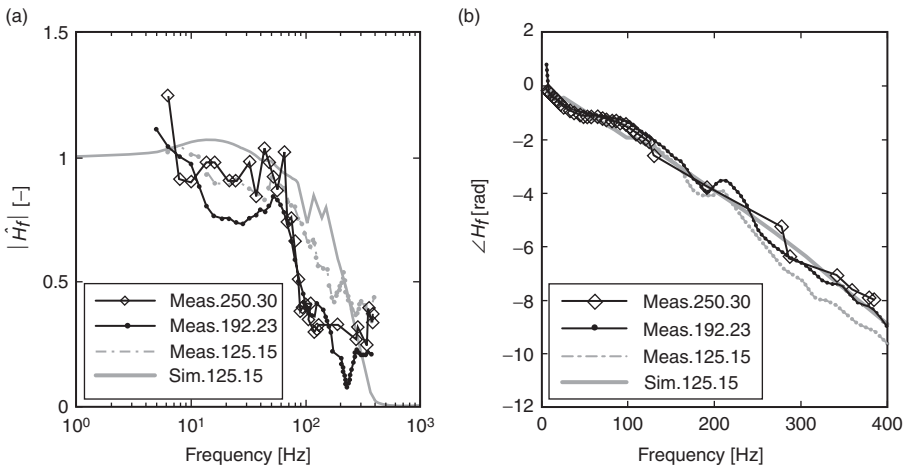

Figure 15: Amplitude and phase of the Flame Transfer Function at operating points 192.23 and 250.30 as compared to operating point 125.15 (power to pressure ratio 83 kW/bar): (a) Amplitude and (b) Phase.

It should be mentioned that the coherence of the measured FTF at operating point 250.30 is much worse than at 125.15 and 192.23. Due to the increased turbulence levels, more noise is present in the system which makes it harder to distinguish the correlated flame response from the uncorrelated flow noise. Therefore, as a result of a too low coherence, about 58% of the measured data has been removed from the data set. These removed data points were located mainly in the higher frequency region, as can be clearly seen in the phase plot in figure 15(b). Consequently, the frequency resolution is low in this region.

From the amplitude of the FTFs it is seen that the level of the FTF of cases 250.30 and 192.23 rolls off faster than the lower pressure case 125.15. Nevertheless, the cut-off frequencies of the cases are approximately similar. An explanation for this could be a change in the form of local flame response as a function of the time delay from the excitation location, which can be caused by a change in the reaction rate with the pressure. Since the simulation results did not show this behaviour, this hypothesis could not be verified.

Another difference between the considered operating points is seen in the phase of the FTF (see figure 15(b)). While the velocities are equal for the three cases, the time delay at higher pressures is less. A possible explanation for this is that the flame moves somewhat closer to the burner at higher pressures for these specifc cases. This could be caused by increased reaction rates at higher pressures (see Warnatz et al. (1996), which brings the flame closer to the burner exit.

It can be summarised that pressure can have a slight influence on the FTF. As a result of higher combustion rate coefficients, the location of the flame can change at higher pressures. Moreover, an increased roll-off of the amplitude of the FTF is noticed at higher pressures.

7. CONCLUSIONS

In this paper, a general approach is presented for measuring the FTF in gas turbine engines and evaluating their thermo-acoustic stability with it. The method for measuring the FTF is completely based on acoustic measurements, i.e. visual access or acoustic modelling is not necessary. This enables the application of the method to existing engines in which some form of excitation to the fuel supply is possible.

The approach for measuring the FTF makes use of a measured spectrum shape of the acoustic flame source in the unperturbed turbulent combustion situation. This measurement of autonomous combustion noise provides an acoustic finger print of the combustor system. Subsequently a test with forced fuel flow oscillations and one microphone provides the necessary information to determine the Flame Transfer Function.

The test rig of a generic combustor (the UT-DESIRE setup) is used to measure the FTF with the proposed method. The rig is operated at power to pressure ratios 100 and 83 kW/bar, and pressures ranging between 1 and 3 bar. The effect of pressure and power is investigated. The method is thereby demonstrated and results are compared to numerical precitions. The measured FTFs agree well with the FTFs from the numerical

CFD simulations. Some characteristics of measured high pressure behavior are not observed in the numerical simulations. This is an indication to improve the high pressure flame modeling.

The measurements and the simulations show an approximately linear frequency dependence of the phase. This indicates that a constant (convective) time delay exists between the excitation and the response. A time delay of 3–4 ms is measured. The time delay decreases with power and can partly be explained from the higher convection velocities with increasing power. However, the measurements show a decrease of the time delay which is less than proportional with the increase of power.

The transfer function amplitude shows a typical low-pass filter behaviour, with a characteristic cut off frequency. Remarkable is an amplitude peak at the cut off frequency.

Measurements at elevated pressures show effects of the mean pressure on the FTF. There is a steeper roll-of in the amplitude and a decrease in the phase shift of the FTF with increasing pressure at constant power to pressure ratio. This is not predicted in the numerical simulations. A plausible explanation for these effects is the increasing reaction rate with the pressure, changing the position and shape of the flame. Remarkable is, that the cut off frequency in the FTF amplitude can not be observed to change with pressure.

ACKNOWLEDGEMENT

This work is performed in the framework of the EU supported project DESIRE, which includes the following partners: Siemens (coordinator), DLR, CERFACS, KEMA, CIMNE, E.ON and the University of Twente.

REFERENCES

Arana, C.A,. B. Sekar, M.A. Mawid, and C.B. Graves. Determination of thermoacoustic response in a demonstrator gas turbine engine. Journal of Engineering for Gas Turbines and Power, 124: pp 46–57, 2002.

Balachandran, R., A.P. Dowling, and E. Mastorakos. Response of turbulent premixed flames subjected to inlet velocity and equivalence ratio perturbations. In Proceedings of the European Combustion Meeting 2005, 2005.

G. Cabot, D. Vauchelles, B. Taupin, and A. Boukhalfa. Experimental study of lean premixed turbulent combustion in a scale gas turbine chamber. Experimental Thermal and Fluid Science, 28, pp 683–690, 2004.

Cheung, W.S., G.J.M. Sims, R.W. Copplestone, J.R. Tilston, C.W. Wilson, S.R. Stow, and A.P. Dowling. Measurement and analysis of flame transfer function in a sector combustor under high pressure conditions. Proceedings of ASME TURBO EXPO 2003, 2003-GT-38219, pp 1–8, 2003.

Cho J.H., T.C. Lieuwen. Modeling the response of premixed flames to mixture ratio perturbations. ASME Paper GT2003-38089, 2003.

Crighton, D.G., A.P. Dowling, J.E. Ffowcs Williams, M. Heckl, and F.G. Leppington. Modern methods in analytical acoustics. Springer-Verlag, London, 1992.

Dawson, S., J.A. Fitzpatrick. Measurement and analysis of thermoacoustic oscillations in a simple dump combustor. Journal of Sound and Vibration, 230(3): pp 649–660, 2000.

Elsari, M. and A. Cummings. Combustion oscillations in gas fired appliances: Eigen-frequencies and stability regimes. Applied Acoustics, 64: pp 565–580, 2003.

Gentemann, A,. C. Hirsch, K. Kunze, T. Sattelmayer, and W. Polifke, Validation of flame transfer function reconstruction for perfectly premixed swirl flames. In Proceedings of ASME Turbo Expo 2004. GT2004-53776, 2004.

Herlufsen, H.. Dual Channel FFT Analysis (Part 1). Number 1 in Technical Review. Bruel & Kjaer, 1984.

Hobson, D.A., J.E. Fackrell, and G. Hewitt, Combustion instabilities in industrial gas turbines {Measurements on operating plant and thermoacoustic modeling, In Proceedings of the ASME Gas Turbine Conference, 1999, ASME paper 99-GT-110, 1999 (American Society of Mechanical Engineers, New York, 1999.

Hubbard, S. and Dowling, A.P. Acoustics resonances of an industrial gas turbine combustion system Transactions of the ASME, Journal of Engineering for Gas Turbines and Power, 123 (4). pp. 766-773, 2001.

Huls, R.A., Acousto-elastic interaction in combustion chambers. PhD thesis, University of Twente, Enschede, 2006.

Kok, J.B.W., Jager, B. de, Modeling of combustion noise in turbulent, premixed flames, technical paper GT2006-90567, ASME IGTI Turbo expo Barcelona, 2006.

Kampen, J.F. van, J.B.W. Kok, and Th.H. van der Meer. One-dimensional acoustic modelling of thermoacoustic instabilities. In Tenth International Congress on Sound and Vibration, 2003.

Kampen, J.F. van, J.B.W. Kok, and Th.H. van der Meer. Prediction of thermo-acoustic spectra in gas turbine combustors using unsteady RaNS CFD simulations. In Eleventh International Congress on Sound and Vibration, pp 3477–3484, 2004.

Kampen, J.F. van, Acoustic pressure oscillations induced by confined turbulent premixed natural gas flames, PhD thesis University of Twente, Enschede, 2006.

Kampen, J.F., Kok, J.B.W., Meer, Th.H. van der, efficient retrieval of the thermo-acoustic flame transfer function from a linearised CFD simulation of a turbulent flame, Int J Numer. Meth Fluids, 54: pp 1131–1149, 2007.

Kleinlugtenbelt, J.H., Acoustic flow oscillations in fuel supply lines, technical report, University of Twente, Enschede, 2005.

Kok, J.B.W., Jager, B. de, The acoustic wave propagation equation in a turbulent combusting flow, Proc. Int. Conf. on Sound & Vibration 14, 9–13 July 2007, Cairns, 2007.

Krüger, U., J. Hüren, S. Hoffmann, W. Krebs, P. Flohr, and D. Bohn. Prediction and measurement of thermoacoustic improvements in gas turbines with annular combustion systems. Journal of Engineering for Gas Turbines and Power, 123(3): pp 557–566, 2001.

Kunze, K., C. Hirsch, and T. Sattelmayer. Transfer function measurements on a swirl stabilized premix burner in an annular combustion chamber. In Proceedings of ASME Turbo Expo 2004. 2004 Power for Land, Sea, and Air. Vienna, Austria, June 14-1, 2004, volume GT2004-53106, 2004.

Lavrentjev, J., Åbom, M., Bodén H., A measurement method for determining the source data of acoustic two-port sources, Journal of Sound and Vibration, 183(3): pp 517–531, 1995.

Lawn, C.J.. Interaction of the acoustic properties of a combustion chamber with those of premixture supply. Journal of Sound and Vibration, 224(5): pp 785–808, 1999.

Lieuwen, T., B.T. Zin. The role of equivalence ratio oscillations in driving combustion instabilities in low NOx gas turbines. In Proceedings of the Twenty Seventh Symposium on Combustion, pp 1809–1816. The Combustion Institute, 1998.

Lieuwen, T.C., Experimental investigation of limit-cycle oscillations. Journal of Propulsion and Power, 18: pp 61–67, 2002.

Mahan, J.R., A. Karchmer, and H.H. Hubbard (editor). Aeroacoustics of Flight Vehicles, Theory and Practice{Volume 1: Noise Sources, chapter Combustion and core noise, pp 483-517. NASA Reference Publication 1258, 1991.

Ng, W.B., K.J. Syed, and Y. Zhang. The study of °ame dynamics and structures in an industrial-scale gas turbine combustor using digital data processing and computer vision techniques. Experimental Thermal and Fluid Science, 29: pp 715–723, 2005.

Paschereit, C.O., B. Schuermans, W. Polifke, and O. Mattson. Measurement of transfer matrices and source terms of premixed flames. Journal of Engineering for Gas Turbines and Power, 124: pp 239–247, 2002.

Rajaram, R., T. Lieuwen. Parametric studies of acoustic radiation from premixed flames. Combustion Science and Technology, 175(12): pp 2269–2298, 2003.

Richards, G.A., M.C. Janus, Characterization of oscillations during premix gas turbine combustion. ASME J. Eng. Gas Turbines Power 120: pp 294–302, 1998.

Sengissen, A.X., Poinsot, T.J., Kampen, J.F. van, Kok, J.B.W., Response of a swirled non-premixed burner to fuel flow rate modulation, in: Lecture Notes in Computational Science and Engineering, vol 56: “Complex effects in Large Eddy Simulation”, Springer, Berlin, pp 337–351, 2007.

Sengissen, A.X., Kampen, J.F. van, R.A. Huls, G.G.M. Stoffels, Kok, J.B.W., Poinsot, T.J., LES and experimental studies of cold and reacting flow in a swirled partially remixed burner with and without fuel modulation, Comb & Flame vol 150, pp 40–53, 2007.

Terao, M., Sekine, H., In-duct pressure measurements to determine sound generation, characteristic reflection and transmission factors of an air moving device in air flow, InterNoise 89, pp 143–146, 1989.

Warnatz, J., U. Maas, and R.W. Dibble, Combustion, Springer-Verlag, Berlin, 1996.

Weigand, P., X.R. Duan, W. Meier, U. Meier, M. Aigner, and C. B´erat, Experimental investigations of an oscillating lean premixed CH4/air swirlflame in a gas turbine model Combustor, Proceedings of the European Combustion Meeting 2005, 2005.

APPENDIX 1. MEASUREMENT OF PRESSURE OSCILLATIONS

Pressure transducers of the type Kulite XCS-190 are used in the setup. For combustion purposes, the transducers' maximum temperature of 175 °C is relatively low. Moreover the static pressure should be compensated in order not to burst the membrane of the transducers at elevated mean pressures (the burst pressure is 1050 mbar). Both of these aspects will be discussed in this appendix.

To enable the Kulite to measure acoustic pressure perturbations at elevated mean pressures, the mean pressure is compensated by imposing this pressure to the rear side of the membrane. The back pressure is supplied through a flexible Teflon hose with an inner diameter of 0.8 mm. The hose is cut to a length of 2 metres and connected to a volume, which is connected to the combustor via a hose with an inner diameter of 8 mm. A larger diameter hose is used for this last part to make sure that the pressure in the volume can follow the pressure in the combustor fast enough. The combination of a volume (area transitions) and the small diameter hose (viscothermal acoustic damping) minimises the acoustic energy transmitted from the combustor to the rear of the membrane of the sensor. Additionally, extra acoustic damping can be expected due to the flexible walls of the Teflon hose. Experimental proof for this is given by Huls (2006).

To remain below their temperature limit, the transducers are mounted flush with a so-called acoustic transmission tube (see figure 4). In this transmission tube, the air is stagnant. Hence, the heat from the hot air in the combustor is transported to the sensor by conduction, which is a relatively slow process. To take away the conducted heat, the transmission tube is cooled from the outside by a fan. When the transmission tube is closed immediately downstream of the pressure transducer, standing waves distort the measured pressure signal at the Kulite. In other words, the measured pressure does not correspond to the pressure in the combustor. To correct this, an anechoic closed end is created by elongating the acoustic transmission tube by a hose of several metres. The last 1.5 metre of this hose is filled with acoustic damping material.

For the auto-spectrum measurements with the pressure transducers, some precautions must be taken to remove the flow noise from the measured signal. When a noise free reference measurement is available, uncorrelated flow noise can be removed by calculating the auto-spectrum at sensor 1 as proposed by Terao and Sekine (1989) and Lavrentjev et al. (1995) (also used by Schuermans et al. (2004) in combustion applications):

$$S_{11} = \frac{S_{12}.S_{21}}{S_{22}} = \frac{S_{12}.S^*_{12}}{S_{22}} \qquad \text{(A1)}$$

where S_{12} is the cross-spectrum between pressure transducers 1 and 2, and the superscript "*" indicates the complex conjugate. In equation A.1, sensor 2 is the noise free reference measurement. Using this equation, only the part of the auto-spectrum of sensor 1 that is correlated with the signal measured by sensor 2 is selected. In case of

the FTF measurements, the excitation of the flame is done with a pulsator. This excitation is noise free and is used for the reconstruction of the auto-spectrum using equation A.1.

Without active perturbation of the flame, the auto-spectrum measured by a transducer mounted at a different location is used for the reconstruction of the auto-spectrum of sensor 1 in equation A.1. To minimise the influence of flow noise, the spacing between the sensors used in the reconstruction is preferably large. Nevertheless, flow noise that is produced at specific locations in the combustor, for instance at the burner exit, can still distort the auto-spectrum measurement. This flow noise is measured by all transducers in the combustor, and is therefore identified as a correlated sound source. However, flow noise is typically a quadrupole type of noise source, while the equivalent source of the flame (heat release rate) is a monopole sound source. For low Mach number flows, the contribution of quadrupole sound sources to the total measured sound is generally much less than the contribution of the monopole sound source resulting from the combustion process. So when the uncorrelated noise (for example flow noise that is produced at the location where each sensor is mounted to the combustor) is removed with equation A.1, the remainder of the measured sound consists mainly of the sound produced by the flame. Nonetheless, care must be taken when interpreting the auto-spectra in the lower frequency range, where the source strength of flow noise is strongest.

APPENDIX 2. EQUIVALENCE RATIO FLUCTUATIONS

In gas turbine combustion systems the ratio of fuel to air mass flow is often characterized by the (fuel) equivalence ratio. This is the actual ratio of fuel to air mass flow, normalized with the ratio necessary for stoichiometric combustion of the fuel:

$$\phi = \frac{m_f / m_{air}}{\left(m_f / m_{air} \right)_{stoichio}} \tag{A2.1}$$

In a (partially) premixed gas turbine combustor, the main mechanism inducing combustion instability is assumed to be a feedback leading to equivalence ratio fluctuations at the location where fuel and air are mixed. However, no direct measurement of the flame transfer function between the flame acoustic source Q' and the equivalence ratio fluctuation ϕ' is available. Instead, the FTF between Q' and the fuel mass flow perturbation m_f'. is measured. In a practical combustion system, perturbing the fuel mass flow also modifies in case of thermo acoustic feed back, the air mass flow at the location where fuel and air are mixed. This is due to the thermo-acoustic source of the flame as a response to the fuel mass flow perturbation. This acoustic source couples back to the mixing location, where it causes an additional perturbation in the air mass flow. In the general situation, the equivalence ratio perturbation resulting from a fuel mass flow fluctuation and/or air mass flow fluctuation can be derived as:

$$d\phi = \frac{1/\dot{m}_{air}}{\left(\dot{m}_f/\dot{m}_{air}\right)_{stoichio}}\left(d\dot{m}_f - \frac{\dot{m}_f}{\dot{m}_{air}}d\dot{m}_{air}\right) = \frac{1/\dot{m}_{air}}{\left(\dot{m}_f/\dot{m}_{air}\right)_{stoichio}}\left(d\dot{m}_f - \frac{\dot{m}_f}{\dot{m}_{air}}d\dot{m}_{air}\right) \quad \text{(A2.2)}$$

$$\frac{\phi'}{\bar{\phi}} = \frac{1}{\bar{\dot{m}}_f}\dot{m}'_f - \frac{1}{\bar{\dot{m}}_{air}}\dot{m}'_{air} \quad \text{(A2.3)}$$

Neglecting this indirect air mass flow fluctuation, the equivalence ratio perturbation resulting from a fuel mass flow fluctuation can be derived as:

$$\frac{\phi'}{\bar{\phi}} \approx \frac{1}{\bar{\dot{m}}_f}\dot{m}'_f \quad \text{(A2.4)}$$

Using this relationship and therewith neglecting the thermoacoustically induced air mass flow fluctuation, it has been shown by LES simulations that a 20% error is made , see Sengissen et al. (2005), depending on the considered frequency. Accepting this error and using equations (7) and (A2.4), the measured transfer function can be transformed to the following transfer function:

$$\frac{\dot{Q}'}{\bar{\dot{Q}}} = H_f\frac{\dot{m}_f'}{\bar{\dot{m}}_f} + H_{air}\frac{\dot{m}_{air}'}{\bar{\dot{m}}_f} \approx H_f\frac{\dot{m}_f'}{\bar{\dot{m}}_f} = H_f\frac{\phi'}{\bar{\phi}} \quad \text{(A2.5)}$$

Or rewriting to the ratio of fluctuation of heat released to fluctuation of equivalence ratio:

$$\frac{\dot{Q}'}{\phi'} = H_f\frac{\bar{\dot{Q}}}{\bar{\phi}} \quad \text{(A2.6)}$$

which can be coupled to the acoustic model. The purpose of transforming the measured transfer function is that the effect of air mass flow fluctuations can be accounted for in the thermo-acoustic network model, since a transfer function involving the equivalence ratio is available.